Organic & Biomolecular Chemistry

ROYAL SOCIETY OF CHEMISTRY

PAPER

View Article Online
View Journal

Cite this: DOI: 10.1039/d1ob02026a

Cross-conjugation controls the stabilities and photophysical properties of heteroazoarene photoswitches†

Daniel M. Adrion and Steven A. Lopez *

Received 15th October 2021,
Accepted 24th December 2021

DOI: 10.1039/d1ob02026a

rsc.li/obc

Azoarene photoswitches are versatile molecules that interconvert from their *E*-isomer to their *Z*-isomer with light. Azobenzene is a prototypical photoswitch but its derivatives can be poorly suited for *in vivo* applications such as photopharmacology due to undesired photochemical reactions promoted by ultraviolet light and the relatively short half-life ($t_{1/2}$) of the *Z*-isomer (2 days). Experimental and computational studies suggest that these properties (λ^{max} of the *E* isomer and $t_{1/2}$ of the *Z*-isomer) are inversely related. We identified isomeric azobisthiophenes and azobisfurans from a high-throughput screening study of 1540 azoarenes as photoswitch candidates with improved λ^{max} and $t_{1/2}$ values relative to azobenzene. We used density functional theory to predict the activation free energies and vertical excitation energies of the *E*- and *Z*-isomers of 2,2- and 3,3-substituted azobisthiophenes and azobisfurans. The half-lives depend on whether the heterocycles are π-conjugated or cross-conjugated with the diazo π-bond. The 2,2-substituted azoarenes both have $t_{1/2}$ values on the scale of 1 hour, while the 3,3-analogues have computed half-lives of 40 and 230 years (thiophene and furan, respectively). The 2,2-substituted heteroazoarenes have significantly higher λ^{max} absorptions than their 3,3-substituted analogues: 76 nm for azofuran and 77 nm for azothiophene.

Introduction

Photoswitches are molecules that are reversibly and chemically interconverted between two states with light. Azobenzene is the most widely studied photoswitch and has a well-documented synthesis *via* diazonium coupling reactions. Azobenzene has been synthesized using cross-coupling reactions,[1–3] nucleophilic aromatic substitution,[4] Bayer–Mills reactions,[5,6] and diazonium coupling.[7] The relatively small size of azobenzene, along with the significant chemical and structural changes resulting from isomerization, has enabled its use for the spatiotemporal control of proteins, lipids, neurotransmitters, neurons, and carbohydrates.[8–20] Phenyl functionalization can improve photophysical properties for applications in chemical biology[21,22] and materials science.[23–27] Scheme 1 shows the photochemical $E \rightarrow Z$ conversion of azobenzene and the subsequent $Z \rightarrow E$ reversion, which can occur thermally or photochemically. Azobenzene requires ultraviolet light (320 nm) to promote the $E \rightarrow Z$ isomerization, limiting its utility *in vivo* due to undesired light-promoted dimerizations, destruction of living tissue from UV-light, and low light penetrability in living tissue.[17,28,29] Further, the meta-stable *Z*-isomer thermally reverts to the *E*-isomer and has a half-life ($t_{1/2}$) of 2 days at room temperature in acetonitrile. This relatively short half-life results in an unstable photostationary state (PSS), thus limiting photoswitch efficacy where bistability is needed.[14] As such, an ideal photoswitch features a long-lived $t_{1/2}$ (*e.g.*, weeks to months), an *E*-isomer λ^{max} in the visible range of the electromagnetic spectrum, and well-separated λ^{max} values for the *E* and *Z* isomers to prevent bimodal isomerization.

Woolley has shown how to tune the properties of azobenzenes through functionalizing the phenyl rings.[17] They have shown how the λ^{max} can be redshifted such that the azoarene will undergo photoswitching under visible light and in physio-

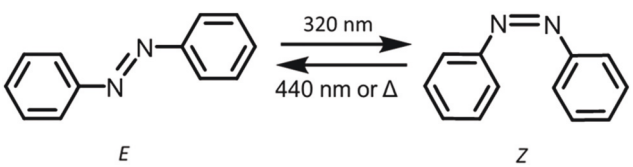

Scheme 1 The azobenzene photoswitch reaction. The $E \rightarrow Z$ isomerization (top) occurs photochemically under UV light. The $Z \rightarrow E$ reversion (bottom) occurs thermally or photochemically under visible light.

Department of Chemistry and Chemical Biology, Northeastern University, Boston, Massachusetts, 02115, USA. E-mail: s.lopez@northeastern.edu

†Electronic supplementary information (ESI) available. See DOI: 10.1039/d1ob02026a

logical conditions.[24,30,31] Since the early 2000s, there has been an effort to design an ideal azoarene photoswitch substituted with aryl groups other than phenyl rings. Reports have shown that the λ^{max} can be redshifted into the visible range by replacing phenyl groups with heteroaryl rings (benzodioxanes,[32] diazinines,[31] pyrroles,[33] pyrazoles[34,35] and imidazoles[36–39]) and by functionalizing the aryl groups.[32,40–54] These heteroazoarenes have relatively high $E \rightarrow Z$ photochemical reaction yields, ranging between 46–98%, and *Z*-isomer half-lives ranging from 1 second up to 46 years. The range in *E*-isomer λ^{max} for these heteroazoarenes is 310–720 nm, pushing them deep into the visible light range. There is an inverse relationship between λ^{max} and $t_{1/2}$ for these heteroazoarenes, those with the highest $t_{1/2}$ have the smallest λ^{max}. Scheme 2 shows heteroazoarenes with heteroaryl rings, and the heteroazoarenes of each type with the longest $t_{1/2}$ values are shown in Fig. 1. Thermal $Z \rightarrow E$ isomerization reactions can proceed through inversion or rotation mechanistic pathways.[55–58] Past computational studies have found that the inversion mechanism is generally preferred for azoarene thermal $Z \rightarrow E$ isomerization reactions.[46,56–61]

Thiophene-containing heteroazoarenes have well-separated *E* and *Z* absorption bands and a high yield of *Z*-isomer for the $E \rightarrow Z$ photoisomerization reaction (94–98%). 2-*hemi*-azothiophene and its derivatives have been studied by Wegner, Dreuw, and Wachtveitl[44,45] (Scheme 2b), and two (3,3) bis-azothiophenes (Fig. 1) have been studied by Perry.[62] The unsubstituted 2-*hemi*-azothiophene (Scheme 2b, left) has a *Z*-isomer $t_{1/2}$ of 7 hours in acetonitrile. Wegner and Heindl[44] showed that electron-donating groups (EDG) at the phenyl *para* position (Me and OMe groups) of 2-*hemi*-azothiophenes lower the $t_{1/2}$ of the *Z*-isomer to 0.5 and 1.9 hours (methyl and methoxy substituent, respectively). Electron withdrawing groups (EWGs) increase the $t_{1/2}$ to 14.3 and 17.8 hours (CF_3 and CN, respectively). Substitution of the thiophene ring with an electron-donating group (OMe) lowered the $t_{1/2}$ to 2.8 hours. Installing push–pull substituents (OMe and CN groups) on an azothiophene lowered the $t_{1/2}$ to 9 minutes. The λ^{max} is 365 nm for the unsubstituted *hemi*-azothiophene and 405 nm for the push–pull *hemi*-azothiophene. All *hemi*-thiophene *E*-isomer λ^{max} values are red-shifted towards the visible range, an improvement over azobenzene. Fig. 1 shows the heteroazoarenes photoswitches of each type with the longest measured half-lives.

Although recent studies have increased the *Z*-isomer $t_{1/2}$ or the *E* isomer λ^{max}, experimental and theoretical studies on heteroazoarenes generally show an inverse relationship between $t_{1/2}$ and λ^{max}.[42,63–65] The reason for this relationship has not been well defined; there is no clear connection between how the *E*-isomer λ^{max} relates to the *Z*-isomer half-life. We have computed the thermal and photophysical properties of four

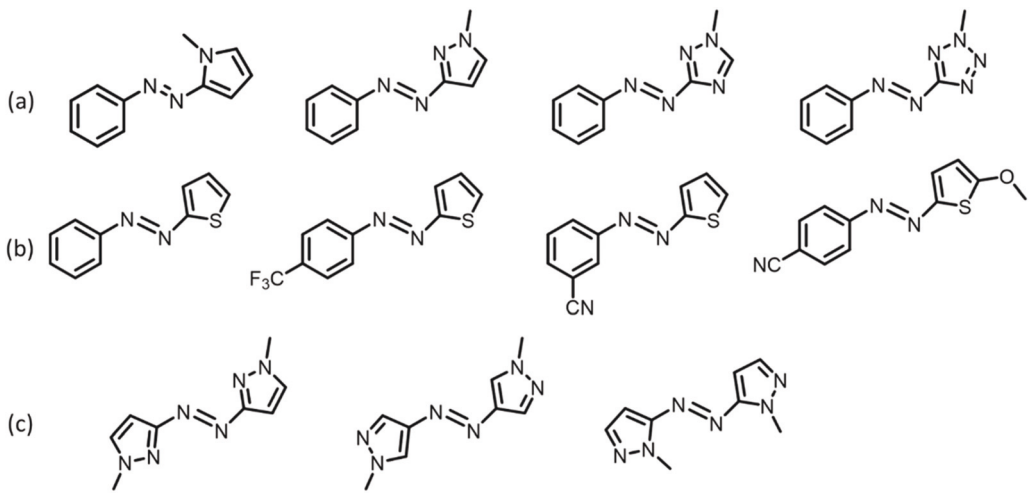

Scheme 2 (a) Nitrogen-containing azoarene photoswitches studied by Fuchter. (b) *Hemi*-azothiophene photoswitches studied by Wegner and Heindl. (c) Azobispyrazole photoswitches synthesized and studied by Li.

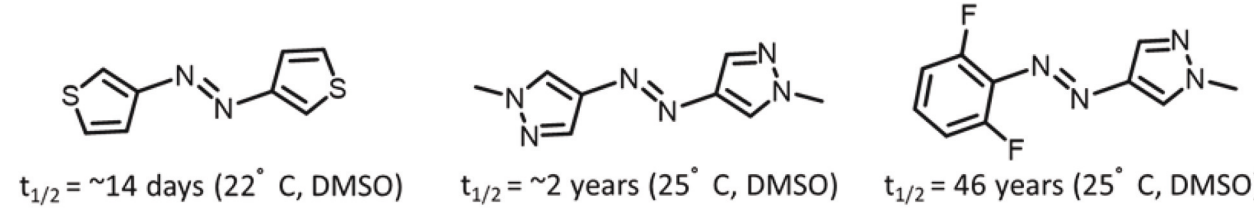

Fig. 1 Three azoarene structures developed by Perry and co-workers (left), Li and co-workers (center), and Fuchter and co-workers (right). Experimental half-lives are provided, along with experimental conditions.

isomeric bis-heteroazoarene photoswitches (two azobisfurans and two azobisthiophenes) using density functional theory (DFT) and time-dependent density functional theory (TD-DFT). The *Z*-isomers of **1**, **2**, **3**, and **4** are shown in Fig. 2. Watchtveitl and co-workers initially reported derivatives of **3-*Z***.[44,45] The (3,3)-azobisthiophene (**4**) and one derivative with ester groups substituted at the 2-position were synthesized and had their UV/Vis spectra and *Z*-isomer half-lives measured by Perry and co-workers.[62] These molecules had $t_{1/2}$ and λ^{max} values of 38 days and 316 nm (unsubstituted azothiophene) and 14 days and 350 nm (ester-substituted azothiophene).

The four heteroazoarenes presented in this study (**1**, **2**, **3**, and **4**) were obtained from the results of a high-throughput virtual screening (HVTS) study, which generated 1540 azoarenes for the VERDE materials database.[66] We calculated the λ^{max} and $t_{1/2}$ values for all molecules, which highlighted the 77 and 76 nm difference in λ^{max} and 10^6 range in half-lives for the structures presented in this study. We also highlight the cross-conjugated π-systems in **2** and **4**. Cross-conjugated molecules have incomplete π-delocalization, causing there to be two isolated π-systems in a molecule instead of one fully delocalized system. Cross-conjugation impacts photophysical properties by increasing the HOMO–LUMO gap, which decreases λ^{max}. Schmidt and co-workers showed that cross-conjugated diynes have lower λ^{max} values than fully conjugated diynes by up to 39 nm because the frontier molecular orbitals are not fully delocalized.[67] Krenske and co-workers demonstrated that thiol nucleophilic additions were accelerated when the enones were cross-conjugated.[68] Sherburn accessed dendralenes with cross-coupling chemistry and found enhanced reactivity towards dienophiles in Diels–Alder reactions. Cross-trienamines were used in asymmetric organocatalysis by Jorgensen and co-workers; experiments and computations demonstrate that relatively high-lying HOMOs increase the cycloaddition reactivity towards oxindoles and azlactones.[69,70] Cross-conjugated trienamines have also been used to enantioselectively access polycyclic natural products such as Lycopladine,[71] bisorbicillinoids,[72] and sesquiterpenes.[73]

Results and discussion

High-throughput screening process

The initial screening of azoarenes was carried out using the high-throughput screening workflow highlighted in an earlier paper from our group.[66] An initial set of azoarenes used included an unsubstituted azobenzene molecule, along with azothiophene, azofuran, and azopyrrole. These molecules are presented in Scheme 3.

Using the substitution patterns from the workflow, we generated 1540 molecules for initial screening, and measured their λ^{max}. From this initial screening, we observed a large difference in the λ^{max} of positional isomers **1** and **2**, and **3** and **4**. Next, we calculated the thermal free energy barriers for the

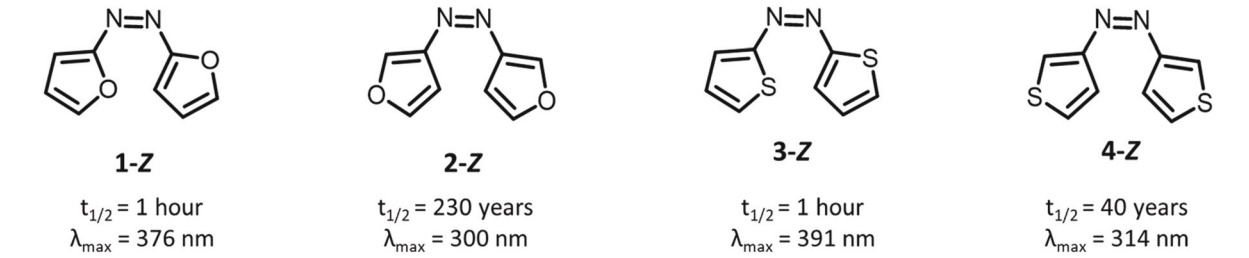

Fig. 2 Four heteroazoarenes considered for this study and their calculated $t_{1/2}$ and λ^{max} values.

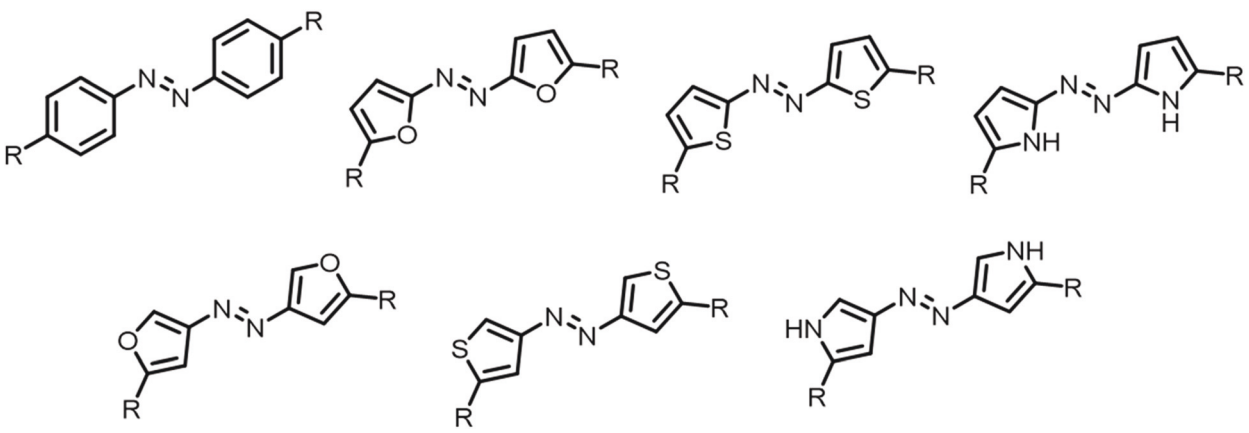

Scheme 3 Molecules used for the initial high-throughput screening.

$Z \rightarrow E$ thermal isomerization reaction for the two sets of positional isomers. These results highlighted the differences in $t_{1/2}$ between the (2,2) (**1** and **3**) and (3,3) (**2** and **4**) azoarenes.

We performed IRC calculations and geometry optimizations to obtain the reactive conformers for the lowest energy transition states of azofurans **1-TS** and **2-TS**, and azothiophenes **3-TS** and **4-TS**. Fig. 3 shows the optimized reactants **1-*Z*** and **2-*Z***, along with their optimized transition structures **1-TS** and **2-TS**, and Fig. 4 shows the energies and geometries of transition structures of **(3–4)-*Z***, **(3–4)-TS**. **2-*Z*** has an isomerization barrier that is 8.5 kcal mol^{-1} higher than the corresponding azofuran **1-*Z***. We sought to understand how the electronic structures of **(1–4)-*Z*** affect the 10^6-fold range in half-lives. The transition states feature coplanar aryl groups; we quantify this coplanarity with an out-of-plane angle (θ). θ is the angle between two normal vectors to the planes of the aryl rings. We will first discuss the structures of the azofuran reactants **1-*Z*** and **2-*Z***, and inversion $Z \rightarrow E$ transition structures, **1-TS** and **2-TS**. We quantify the differences in geometry between the reactants and transition states by measuring the ring co-planarity (θ) and key bond lengths that describe the changes in π-conjugation. We then compare these structures to **3** and **4** to understand how bisazothiophenes differ from bisazofurans. The frontier molecular orbitals were computed; we discuss how their energies and overlap are affected by cross-conjugation.

The top portion of Fig. 3 shows the optimized reactant geometries **1-*Z*** and **2-*Z***. The C–C bond lengths in the furan rings are 1.37–1.42 Å for **1-*Z*** and 1.35–1.45 Å for **2-*Z***. These distances correspond to aromatic C–C bond lengths. The C–O bonds range from 1.34–1.38 Å for **1-*Z*** and 1.34–1.37 Å for **2-*Z***, all consistent with aromatic C–O bond lengths in furan rings. The two reactants also have the same CNNC dihedral angle (θ = 10°), indicating equivalent relative planarities of the aryl rings in both structures. The N═N π-bonds are 1.27 Å in **1-*Z*** and

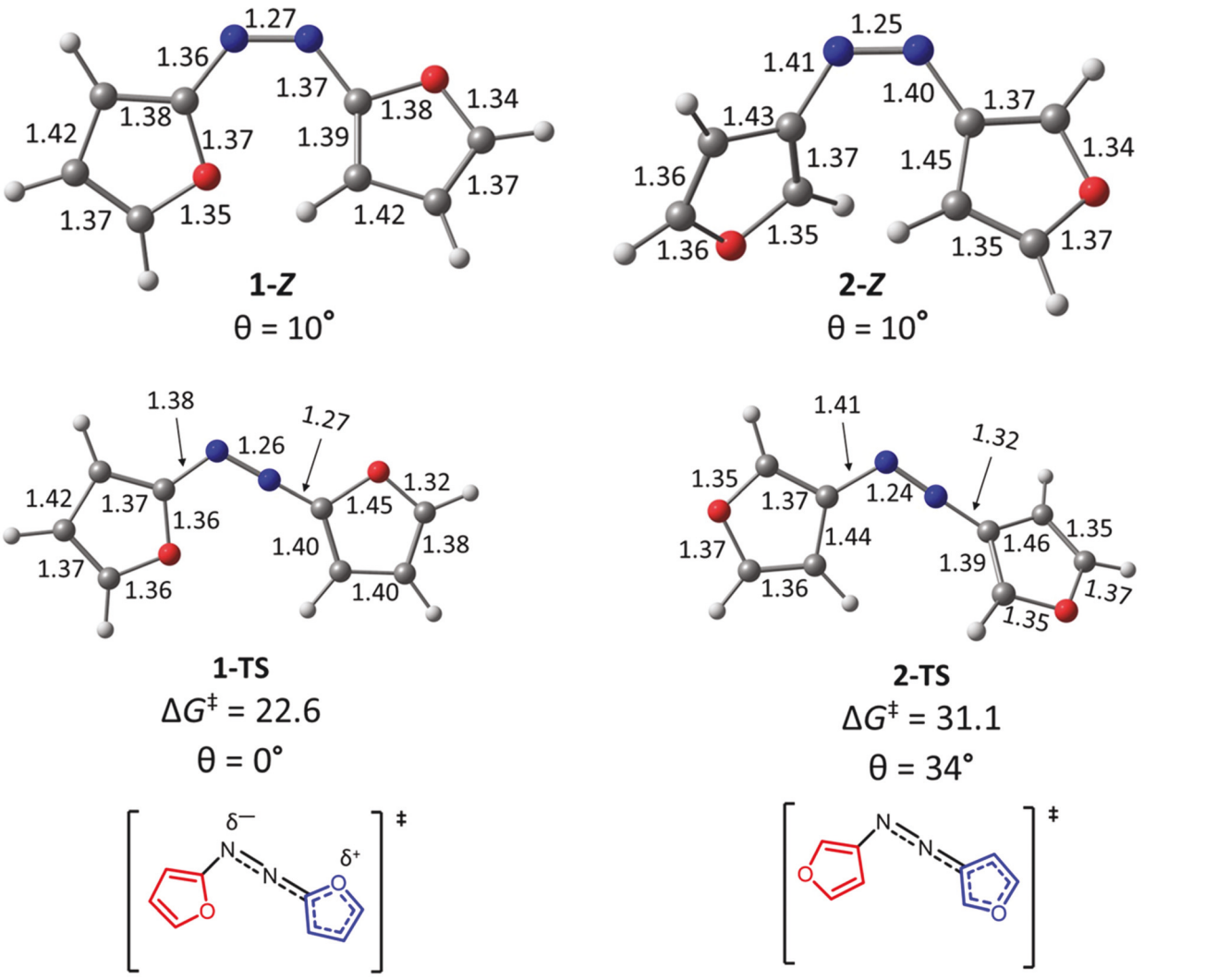

Fig. 3 Top: Optimized azofuran reactive conformers **1-*Z*** (left) and **2-*Z*** (right). Bond lengths are given in Angstroms (Å). The dihedral angle (θ) measures the CNNC angle. Bottom: Computed azofuran transition states **1-TS** (left) and **2-TS** (right). Bond lengths are shown in angstroms (Å). The out-of-plane angle, θ, measures the relative planarity of the furan rings.

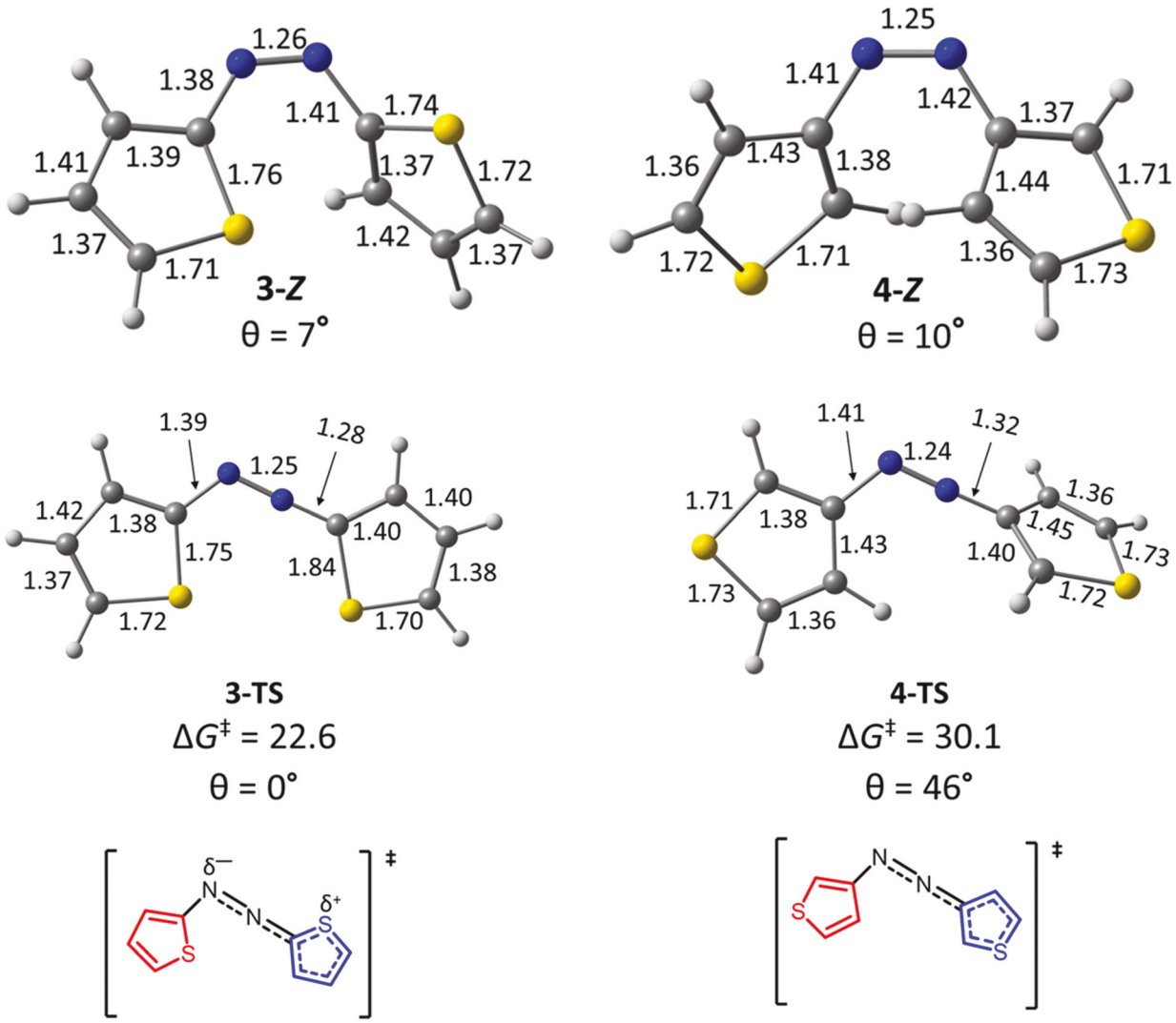

Fig. 4 Top: Optimized azothiophene reactive conformers **3-*Z*** (left) and **4-*Z*** (right). The bond lengths are given in Angstroms (Å). The dihedral angle (θ) measures the CNNC angle. Bottom: Computed azothiophene transition states **3-TS** (left) and **4-TS** (right). Bond lengths are shown in angstroms (Å). The out-of-plane angle, θ, measures the relative planarity of the thiophene rings.

1.25 Å in **2-*Z***. The C–N bonds in **2-*Z*** (1.40 and 1.41 Å) are significantly longer than those of **1-*Z*** (1.36 and 1.37 Å). The C–N bond lengths in **1-*Z*** are consistent with aromatic C–N bond distances, while the C–N bond distances in **2-*Z*** more closely resemble C–N single bonds. The shorter C–N bonds and the longer N=N bond indicate more electron delocalization between the furan rings in **1-*Z*** than **2-*Z***. We now turn our attention to the transition structures, **1-TS** and **2-TS**.

The $\Delta G^{\ddagger}$ for the thermal $Z \rightarrow E$ isomerization of **1-TS** is 22.6 kcal mol^{-1}; the $\Delta G^{\ddagger}$ for the thermal $Z \rightarrow E$ isomerization of **2-TS** is 31.1 kcal mol^{-1}. The difference in activation free energies ($\Delta\Delta G^{\ddagger}$) is 8.5 kcal mol^{-1}, corresponding to half-lives of one hour and 230 years, respectively. **1-TS** and **2-TS** involve a rehybridization of one of the N atoms, which corresponds to a linearization of the NNC2 and NNC3 angles (NNC angles of 179° and 178°, respectively). The N=N diazo bond lengths for **1-TS** and **2-TS** are 1.26 Å and 1.24 Å, respectively. These bond lengths are shorter than in the *Z*-isomers, where they are 1.27 and 1.25 Å for **1-*Z*** and **2-*Z***, respectively.

The C–C bond lengths in the furan rings range from 1.35 to 1.46 Å, consistent with aromatic C–C bond lengths in the crystal structure of furan (1.32 to 1.43 Å). The C–O bonds have a small range in **1-*Z*** (1.34–1.38 Å) but have a larger range in **1-TS** (1.32–1.45 Å). The 1.32 Å C–O bond length is consistent with an aromatic C–O bond. The furan on the left side (red) of **1-TS** has identical C–O bond lengths (1.36 Å), while the furan on the right side (blue) of **1-TS** has C–O bond lengths of 1.32 and 1.45 Å. This disparity is caused by an asymmetric resonance-donation of a furan lone pair orbital in **1-TS** relative to **1-*Z***. The C–N bond lengths flanking the diazo bond are 1.38 Å and 1.27 Å. The C–N bond connecting the blue furan to the N=N bond significantly shortens in **1-TS** from **1-*Z*** (1.27 Å from 1.37 Å), indicating increased π-character, while the other C–N bond is nearly unchanged from **1-TS** to **1-*Z*** (1.38 Å and

1.36 Å, respectively). The relative planarity between the two rings (θ) is significantly different for **1-TS** and **2-TS**. The two furan rings in **1-TS** are fully coplanar ($\theta = 0°$), maximizing the π-conjugation between them. **2-TS** features cross-conjugation, which implies that π-conjugation is limited to the aromatic π-system of the blue furan with the diazo bond throughout the reaction. While **2-TS** also involves a rehybridization of one of the N-atoms, the furans are not coplanar ($\theta = 34°$) because the rings are not electronically communicating through the diazo bond. The difference in the C–O bond lengths in **2-TS** is 0.03 Å (1.35 and 1.38 Å), which suggests that the delocalization of oxygen lone pairs substantially decreases. The C–N bonds flanking the N=N bond are 1.41 and 1.32 Å. As such, azoarenes featuring cross-conjugation are not fully π-delocalized. This decrease in resonance delocalization results in the substantial 8.5 kcal mol^{-1} $\Delta\Delta G^{\ddagger}$ of these isomeric azofurans. Thus, the (2,2)-diazofurans are 10^6-fold more reactive than the (3,3)-diazofurans. We now turn our attention to the azothiophenes **3** and **4**.

The C–C bond lengths in the thiophene rings range from 1.37 to 1.42 Å for **3-*Z*** and 1.36 to 1.44 Å for **4-*Z***. These distances correspond to aromatic C–C bond lengths (1.35 to 1.44 Å in the crystal structure of thiophene). The C–S bond lengths range from 1.71–1.76 Å for **3-*Z*** and 1.71–1.73 Å for **4-*Z***. **3-*Z*** has a CNNC dihedral of 7°; **4-*Z*** has a CNNC dihedral of 10°. The structural differences between the two reactants are present in the bond distances of the CNNC bonds. The N=N bonds are 1.26 Å in **3-*Z*** and 1.25 Å in **4-*Z***. The C–N bonds in **4-*Z*** (1.41 and 1.42 Å) are longer than the analogous bonds in **3-*Z*** (1.38 and 1.41 Å). The shorter C–N bond length in **3-*Z*** is consistent with an aromatic C–N bond, and the longer C–N bond lengths in **4-*Z*** are consistent with single bonds. The shorter C–N bonds and the longer N=N bond indicate that **3-*Z*** has more electron delocalization between the two thiophene rings than **4-*Z***.

The $\Delta G^{\ddagger}$ for **3-TS** is 22.6 kcal mol^{-1}, and the $\Delta G^{\ddagger}$ for **4-TS** is 30.1 kcal mol^{-1}. The difference in activation free energies ($\Delta\Delta G^{\ddagger}$) is 7.5 kcal mol^{-1}, corresponding to half-lives of one hour and 40 years, respectively. Transition structures **3-TS** and **4-TS** involve rehybridization about one of the N atoms and have nearly linear NNC_2 and NNC_3 angles (179° and 178°, respectively). The N=N bonds are shorter in **3-TS** (1.25 Å) and **4-TS** (1.24 Å) relative to their corresponding reactants (1.26 Å and 1.25 Å, respectively). These bond lengths shorten as the azothiophenes reach their respective transition structure geometries, resulting from the rehybridization of one of the N atoms.

The C–C bond lengths in the thiophene rings range from 1.36 to 1.45 Å, which is consistent with aromatic C–C bond lengths in thiophene rings. The C–S bonds are 1.71–1.76 Å in **3-*Z*** but diverge in **3-TS** (1.70–1.84 Å) because one of the sulfur lone pairs is delocalized through the transition structure. This phenomenon results in the zwitterionic electronic structure shown in Fig. 4. The shorter bond length resembles a C–S double bond,[74] while the longer bond corresponds to a broken C–S π-bond (the aromatic C–S bonds in the crystal structure of thiophene are 1.74 Å).[74] The red thiophene ring has two nearly identical C–S bond lengths (with lengths of 1.72 and 1.75 Å), indicating aromatic C–S bond lengths. The C–N bonds flanking the diazo bond differ substantially (1.39 and 1.28 Å) in **3-TS**. The C–N bond connecting the blue thiophene to the N=N bond significantly shortens in **3-TS** from **3-*Z*** (1.28 Å from

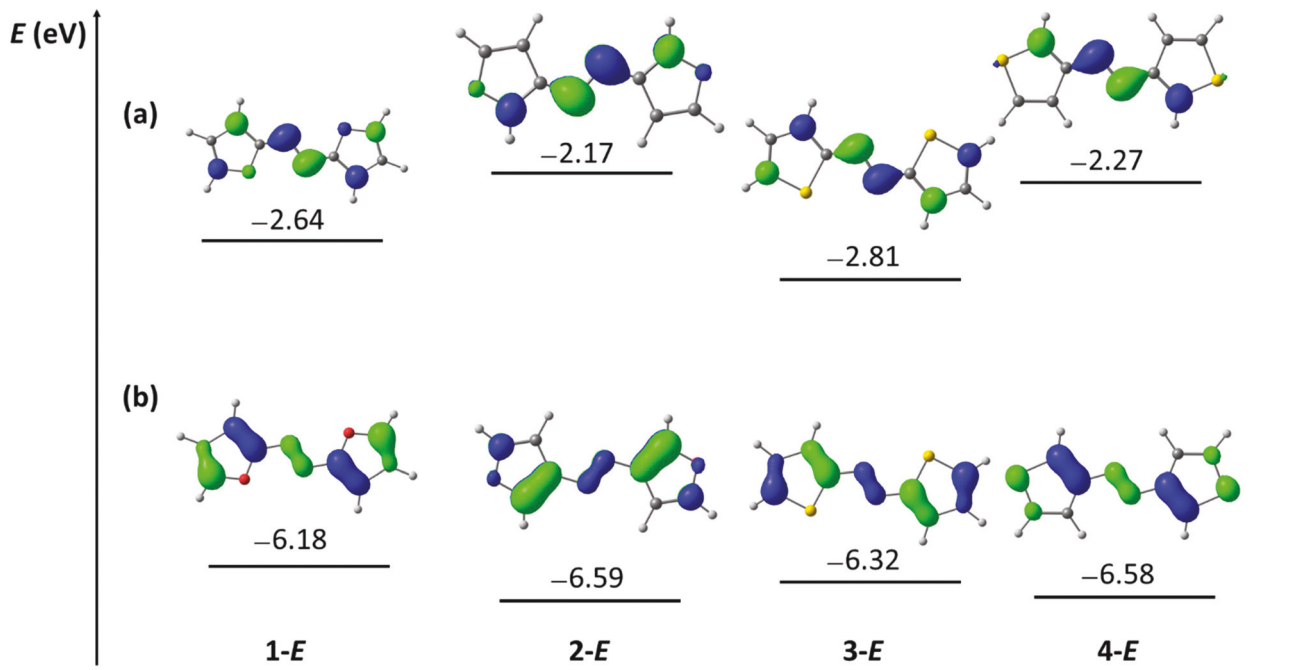

Fig. 5 Computed LUMOs (a) and HOMOs (b) of **1-*E***, **2-*E***, **3-*E***, and **4-*E***. The orbitals were calculated with PBE0-D3(BJ)/6-31+G(d,p) and IEFPCM^{H_2O}.

1.38 Å), indicating increased π-conjugation, while the other C–N bond is relatively unchanged from **3-*Z*** to **3-TS** (1.41 and 1.39 Å, respectively). The thiophene rings of **4-TS** deviate significantly from coplanarity ($\theta = 46°$) due to the decreased conjugation across the diazo bond. The difference in the C–S bond lengths in **4-TS** is 0.02 Å (1.71–1.73 Å), suggesting that the sulfur delocalization effect significantly decreased relative to **3-TS**. The C–N bonds flanking the N=N bond are 1.41 Å and 1.32 Å. These corresponding bond lengths in **3-TS** are shorter (1.39 Å and 1.28 Å) due to increased π-conjugation.

We performed time-dependent density functional theory (TD-DFT) calculations to predict the nature of the electronic transitions and vertical excitation energies of the *E*-isomers. The corresponding λ^{max} derived from the vertical excitation energies of **1-*E***, **2-*E***, **3-*E***, and **4-*E*** are 382, 304, 400, and 317 nm, respectively. All electronic transitions shown below correspond to a single excitation from the HOMO to the LUMO ($\pi \rightarrow \pi^*$). The experimental λ^{max} of (3,3) azothiophene is 332 nm.[62] **1-*E***, and **3-*E*** have λ^{max} which are redshifted by 78 nm and 83 nm relative to **2-*E*** and **4-*E***, respectively. To understand the origin of the 96 nm range in λ^{max} along this series, we computed the frontier molecular orbitals (FMOs) for **1-*E***, **2-*E***, **3-*E***, and **4-*E*** (Fig. 5).

1-*E* and **3-*E*** have fully delocalized π-systems across the diazo bond, while **2-*E*** and **4-*E*** show interrupted π-electron density due to their cross-conjugated nature. The cross-conjugated π-systems in **2-*E*** and **4-*E*** affect the energies and energy gaps of the frontier molecular orbitals (HOMO and LUMO). The delocalization effect in **1-*E*** and **3-*E*** leads to higher-lying HOMOs and lower-lying LUMOs relative to **2-*E*** and **4-*E***, leading to decreased HOMO–LUMO gaps. The HOMO for **1-*E*** is –6.18 eV, 0.41 eV higher than the HOMO for **2-*E*** (−6.59 eV), and the HOMO for **3-*E*** is −6.32 eV, 0.26 eV higher than the HOMO for **4-*E*** (−6.58 eV). The LUMO for **1-*E*** is −2.64 eV, which is 0.47 eV lower than the LUMO for **2-*E*** (−2.17 eV), and the LUMO for **3-*E*** is −2.81 eV, 0.53 eV lower than the LUMO for **4-*E*** (−2.27 eV). The HOMO–LUMO gaps of **1-*E*** and **2-*E*** are 3.54 eV and 4.42 eV (a 0.88 eV difference), and the same gaps are 3.51 eV and 4.31 eV for **3-*E*** and **4-*E***, a difference of 0.80 eV. These results suggest that the cross-conjugated π-systems lead to lower energy HOMO and higher energy LUMO orbitals for azoarene photoswitches, which is consistent with the effects that cross-conjugation has on other molecular systems. The large frontier molecular orbital gaps cause higher vertical excitation energies and smaller λ^{max}.

Conclusion

We have used DFT to determine the photophysical properties and thermal stabilities of four bis-diazoarene photoswitches. We predict that the thermal half-lives of the isomeric *Z*-isomers range from hours to years. The (3,3)-substituted isomers (**2** and **4**) have cross-conjugated π-systems, significantly affecting the photophysical and thermal properties. This truncated π-conjugation leads to large optical gaps, thus requiring UV light for photoswitching (300 nm for **2-*E*** and 314 nm for **4-*E***). Those with fully π-conjugated systems (**1-*E*** and **3-*E***) contain relatively small optical gaps, which enable visible light photoswitching (376 nm and 391 nm, respectively). The extent of π-conjugation strongly influences the transition structures and thermal half-lives of the *Z*-isomers. **1-*Z*** and **3-*Z*** have a small $\Delta G^{\ddagger}$, which translates to a $t_{1/2}$ of one hour. **2-TS** and **4-TS** are higher in energy due to the limited π-delocalization, and the $t_{1/2}$ lifetimes of **2-*Z*** and **4-*Z*** are in the range of 40–230 years. Towards photoswitches with long half-lives and visible-light absorption, we recommend designing photoswitches with two aryl groups, one cross-conjugated and one fully conjugated. For example, an azoarene with a 3-thiophene ring and a *para*-nitrophenyl ring. The strongly withdrawing nature of the nitro group red shifts the λ^{max}, while the cross-conjugation contributes to higher activation free energies and long $t_{1/2}$. We are currently exploring non-symmetric azoarenes with one phenyl ring and one cross-conjugated aryl ring (thiophene or furan) flanking the diazo bond.

Computational methods

We performed DFT calculations to predict the activation free energies ($\Delta G^{\ddagger}$) of (**1–4-*Z***). We computed the structures and energies of the *Z*-isomer, *E*-isomer, and transition structure for each reaction. First, the transition structures were optimized using the *EZ*-TS code recently reported by our group.[75] After locating the lowest energy transition states, we ran intrinsic reaction coordinate (IRC) calculations and optimized the reactive conformers corresponding to the reactant (*Z*-isomer) and product (*E*-isomer) for each thermal $Z \rightarrow E$ isomerization. All calculations were performed using the Gaussian 16 software.[76] The PBE0-D3BJ[77]/6-31+G(d,p)[78] model chemistry was used for all geometry optimizations and frequency calculations. Vertical excitation energies of **1-4-*E*** were calculated using TD-DFT[79] with the ωB97X-D[80]/6-311+G(d,p) model chemistry in IEFPCM^{water}.[81] The first 10 singlet excited states were included in all TD-DFT calculations.

Conflicts of interest

There are no conflicts to declare.

Acknowledgements

D. M. A. and S. A. L. acknowledge Dr Jordan M. Cox (Northeastern), Professor Dirk Trauner, and Dr Bruno Paz (NYU) for helpful discussions and feedback on this work. We thank the National Science Foundation (NSF-OAC-2118201 and NSF-OAC-1940307) for the financial support. D. M. A. and S. A. L. appreciate the assistance from the Northeastern Research Computing Team and access to the computing resources provided by the Massachusetts Life Science Center (Grant G00006360) and the Discovery Cluster.

References

1 Y. Wang, R. Xie, L. Huang, Y.-N. Tian, S. Lv, X. Kong and S. Li, Divergent synthesis of unsymmetrical azobenzenes via Cu-catalyzed C–N coupling, *Org. Chem. Front.*, 2021, **8**(21), 5962–5967.

2 R. Kılınçarslan, E. Erdem and H. Kocaokutgen, Synthesis and spectral characterization of some new azo dyes and their metal complexes, *Transition Met. Chem.*, 2006, **32**(1), 102–106.

3 A. Staubitz, M. Walther, W. Kipke, S. Schultzke and S. Ghosh, Modification of Azobenzenes by Cross-Coupling Reactions, *Synthesis*, 2021, **53**(7), 1213–1228.

4 H. Hartmann, M. Schulze and R. Guenther, Nucleophilic Substitution in Arylazo Phenols - a Simple Route for Preparing Chlorosubstituted Azobenzenes, *Dyes Pigm.*, 1991, **15**, 255–262.

5 A. H. Heindl and H. A. Wegner, Starazo triple switches - synthesis of unsymmetrical 1,3,5-tris(arylazo)benzenes, *Beilstein J. Org. Chem.*, 2020, **16**, 22–31.

6 C. Slavov, C. Yang, L. Schweighauser, C. Boumrifak, A. Dreuw, H. A. Wegner and J. Wachtveitl, Connectivity matters - ultrafast isomerization dynamics of bisazobenzene photoswitches, *Phys. Chem. Chem. Phys.*, 2016, **18**(22), 14795–14804.

7 E. Merino, Synthesis of azobenzenes: the coloured pieces of molecular materials, *Chem. Soc. Rev.*, 2011, **40**(7), 3835–3853.

8 J. Morstein and D. Trauner, Photopharmacological control of lipid function, *Methods Enzymol.*, 2020, **638**, 219–232.

9 M. Doroudgar, J. Morstein, J. Becker-Baldus, D. Trauner and C. Glaubitz, How Photoswitchable Lipids Affect the Order and Dynamics of Lipid Bilayers and Embedded Proteins, *J. Am. Chem. Soc.*, 2021, **143**(25), 9515–9528.

10 M. Korbus, S. Backe and F. J. Meyer-Almes, The cis-state of an azobenzene photoswitch is stabilized through specific interactions with a protein surface, *J. Mol. Recognit.*, 2015, **28**(3), 201–209.

11 L. Albert and O. Vazquez, Photoswitchable peptides for spatiotemporal control of biological functions, *Chem. Commun.*, 2019, **55**(69), 10192–10213.

12 J. B. Trads, K. Hull, B. S. Matsuura, L. Laprell, T. Fehrentz, N. Gorldt, K. A. Kozek, C. D. Weaver, N. Klocker, D. M. Barber and D. Trauner, Sign Inversion in Photopharmacology: Incorporation of Cyclic Azobenzenes in Photoswitchable Potassium Channel Blockers and Openers, *Angew. Chem., Int. Ed.*, 2019, **58**(43), 15421–15428.

13 B. Cheng, J. Morstein, L. K. Ladefoged, J. B. Maesen, B. Schiott, S. Sinning and D. Trauner, A Photoswitchable Inhibitor of the Human Serotonin Transporter, *ACS Chem. Neurosci.*, 2020, **11**(9), 1231–1237.

14 J. Broichhagen, J. A. Frank and D. Trauner, A roadmap to success in photopharmacology, *Acc. Chem. Res.*, 2015, **48**(7), 1947–1960.

15 M. Banghart, K. Borges, E. Isacoff, D. Trauner and R. H. Kramer, Light-activated ion channels for remote control of neuronal firing, *Nat. Neurosci.*, 2004, **7**(12), 1381–1386.

16 F. Hamon, F. Djedaini-Pilard, F. Barbot and C. Len, Azobenzenes—synthesis and carbohydrate applications, *Tetrahedron*, 2009, **65**(49), 10105–10123.

17 A. A. Beharry and G. A. Woolley, Azobenzene photoswitches for biomolecules, *Chem. Soc. Rev.*, 2011, **40**(8), 4422–4437.

18 T. Fehrentz, M. Schonberger and D. Trauner, Optochemical genetics, *Angew. Chem., Int. Ed.*, 2011, **50**(51), 12156–12182.

19 J. Broichhagen, T. Podewin, H. Meyer-Berg, Y. von Ohlen, N. R. Johnston, B. J. Jones, S. R. Bloom, G. A. Rutter, A. Hoffmann-Roder, D. J. Hodson and D. Trauner, Optical Control of Insulin Secretion Using an Incretin Switch, *Angew. Chem., Int. Ed.*, 2015, **54**(51), 15565–15569.

20 L. Laprell, E. Repak, V. Franckevicius, F. Hartrampf, J. Terhag, M. Hollmann, M. Sumser, N. Rebola, D. A. DiGregorio and D. Trauner, Optical control of NMDA receptors with a diffusible photoswitch, *Nat. Commun.*, 2015, **6**, 8076.

21 K. Hull, J. Morstein and D. Trauner, In Vivo Photopharmacology, *Chem. Rev.*, 2018, **118**(21), 10710–10747.

22 I. Tochitsky, M. A. Kienzler, E. Isacoff and R. H. Kramer, Restoring Vision to the Blind with Chemical Photoswitches, *Chem. Rev.*, 2018, **118**(21), 10748–10773.

23 A. A. Beharry, O. Sadovski and G. A. Woolley, Azobenzene photoswitching without ultraviolet light, *J. Am. Chem. Soc.*, 2011, **133**(49), 19684–19687.

24 D. Martinez-Lopez, A. Babalhavaeji, D. Sampedro and G. A. Woolley, Synthesis and characterization of bis(4-amino-2-bromo-6-methoxy)azobenzene derivatives, *Beilstein J. Org. Chem.*, 2019, **15**, 3000–3008.

25 J. Garcia-Amoros and D. Velasco, Recent advances towards azobenzene-based light-driven real-time information-transmitting materials, *Beilstein J. Org. Chem.*, 2012, **8**, 1003–1017.

26 L. N. Lameijer, S. Budzak, N. A. Simeth, M. J. Hansen, B. L. Feringa, D. Jacquemin and W. Szymanski, General Principles for the Design of Visible-Light-Responsive Photoswitches: Tetra-ortho-Chloro-Azobenzenes, *Angew. Chem., Int. Ed.*, 2020, **59**(48), 21663–21670.

27 M. J. Hansen, M. M. Lerch, W. Szymanski and B. L. Feringa, Direct and Versatile Synthesis of Red-Shifted Azobenzenes, *Angew. Chem., Int. Ed.*, 2016, **55**(43), 13514–13518.

28 M. M. Lerch, M. J. Hansen, G. M. van Dam, W. Szymanski and B. L. Feringa, Emerging Targets in Photopharmacology, *Angew. Chem., Int. Ed.*, 2016, **55**(37), 10978–10999.

29 W. Szymanski, J. M. Beierle, H. A. Kistemaker, W. A. Velema and B. L. Feringa, Reversible photocontrol of biological systems by the incorporation of molecular photoswitches, *Chem. Rev.*, 2013, **113**(8), 6114–6178.

30 A. A. Beharry, O. Sadovski and G. A. Woolley, Azobenzene Photoswitching without Ultraviolet Light, *J. Am. Chem. Soc.*, 2011, **133**(49), 19684–19687.

31 S. Samanta, A. Babalhavaeji, M. X. Dong and G. A. Woolley, Photoswitching of ortho-substituted azonium ions by red light in whole blood, *Angew. Chem., Int. Ed.*, 2013, **52**(52), 14127–14130.
32 M. Dong, A. Babalhavaeji, C. V. Collins, K. Jarrah, O. Sadovski, Q. Dai and G. A. Woolley, Near-Infrared Photoswitching of Azobenzenes under Physiological Conditions, *J. Am. Chem. Soc.*, 2017, **139**(38), 13483–13486.
33 P. J. Coelho, L. M. Carvalho, A. M. C. Fonseca and M. M. M. Raposo, Photochromic properties of thienylpyrrole azo dyes in solution, *Tetrahedron Lett.*, 2006, **47**(22), 3711–3714.
34 J. Simke, T. Bosking and B. J. Ravoo, Photoswitching of ortho-Aminated Arylazopyrazoles with Red Light, *Org. Lett.*, 2021, **23**(19), 7635–7639.
35 Y. T. Wang, X. Y. Liu, G. Cui, W. H. Fang and W. Thiel, Photoisomerization of Arylazopyrazole Photoswitches: Stereospecific Excited-State Relaxation, *Angew. Chem., Int. Ed.*, 2016, **55**(45), 14009–14013.
36 C. E. Weston, R. D. Richardson and M. J. Fuchter, Photoswitchable basicity through the use of azoheteroarenes, *Chem. Commun.*, 2016, **52**(24), 4521–4524.
37 T. Wendler, C. Schutt, C. Nather and R. Herges, Photoswitchable azoheterocycles via coupling of lithiated imidazoles with benzenediazonium salts, *J. Org. Chem.*, 2012, **77**(7), 3284–3287.
38 J. Otsuki, K. Suwa, K. Narutaki, C. Sinha, I. Yoshikawa and K. Araki, Photochromism of 2-(Phenylazo)imidazoles, *J. Phys. Chem. A*, 2005, **109**, 8064–8069.
39 J. Otsuki, K. Suwa, K. K. Sarker and C. Sinha, Photoisomerization and Thermal Isomerization of Arylazoimidazoles, *J. Phys. Chem. A*, 2007, **111**, 1403–1409.
40 H. Qian, Y. Y. Wang, D. S. Guo and I. Aprahamian, Controlling the Isomerization Rate of an Azo-BF2 Switch Using Aggregation, *J. Am. Chem. Soc.*, 2017, **139**(3), 1037–1040.
41 Y. Yang, R. P. Hughes and I. Aprahamian, Visible light switching of a BF2-coordinated azo compound, *J. Am. Chem. Soc.*, 2012, **134**(37), 15221–15224.
42 D. B. Konrad, G. Savasci, L. Allmendinger, D. Trauner, C. Ochsenfeld and A. M. Ali, Computational Design and Synthesis of a Deeply Red-Shifted and Bistable Azobenzene, *J. Am. Chem. Soc.*, 2020, **142**(14), 6538–6547.
43 D. B. Konrad, J. A. Frank and D. Trauner, Synthesis of Redshifted Azobenzene Photoswitches by Late-Stage Functionalization, *Chem. – Eur. J.*, 2016, **22**(13), 4364–4368.
44 A. H. Heindl and H. A. Wegner, Rational Design of Azothiophenes-Substitution Effects on the Switching Properties, *Chemistry*, 2020, **26**(60), 13730–13737.
45 C. Slavov, C. Yang, A. H. Heindl, H. A. Wegner, A. Dreuw and J. Wachtveitl, Thiophenylazobenzene: An Alternative Photoisomerization Controlled by Lone-Pairpi Interaction, *Angew. Chem., Int. Ed.*, 2020, **59**(1), 380–387.
46 Y. He, Z. Shangguan, Z. Y. Zhang, M. Xie, C. Yu and T. Li, Azobispyrazole Family as Photoswitches Combining (Near-) Quantitative Bidirectional Isomerization and Widely Tunable Thermal Half-Lives from Hours to Years*, *Angew. Chem., Int. Ed.*, 2021, **60**(30), 16539–16546.
47 J. Calbo, C. E. Weston, A. J. White, H. S. Rzepa, J. Contreras-Garcia and M. J. Fuchter, Tuning Azoheteroarene Photoswitch Performance through Heteroaryl Design, *J. Am. Chem. Soc.*, 2017, **139**(3), 1261–1274.
48 J. Calbo, A. R. Thawani, R. S. L. Gibson, A. J. P. White and M. J. Fuchter, A combinatorial approach to improving the performance of azoarene photoswitches, *Beilstein J. Org. Chem.*, 2019, **15**, 2753–2764.
49 C. E. Weston, R. D. Richardson, P. R. Haycock, A. J. White and M. J. Fuchter, Arylazopyrazoles: azoheteroarene photoswitches offering quantitative isomerization and long thermal half-lives, *J. Am. Chem. Soc.*, 2014, **136**(34), 11878–11881.
50 J. Broichhagen, J. A. Frank, N. R. Johnston, R. K. Mitchell, K. Smid, P. Marchetti, M. Bugliani, G. A. Rutter, D. Trauner and D. J. Hodson, A red-shifted photochromic sulfonylurea for the remote control of pancreatic beta cell function, *Chem. Commun.*, 2015, **51**(27), 6018–6021.
51 S. Crespi, N. A. Simeth and B. König, Heteroaryl azo dyes as molecular photoswitches, *Nat. Rev. Chem.*, 2019, **3**(3), 133–146.
52 P. J. Coelho, C. M. Sousa, M. C. R. Castro, A. M. C. Fonseca and M. M. M. Raposo, Fast thermal cis–trans isomerization of heterocyclic azo dyes in PMMA polymers, *Opt. Mater.*, 2013, **35**(6), 1167–1172.
53 D. Wannipurage, S. S. Kurup and S. Groysman, Heterocoupling of Different Aryl Nitrenes to Produce Asymmetric Azoarenes Using Iron–Alkoxide Catalysis and Investigation of the Cis–Trans Isomerism of Selected Bulky Asymmetric Azoarenes, *Organometallics*, 2021, **40**(21), 3637–3644.
54 Y. Xu, C. Gao, J. Andréasson and M. Grøtli, Synthesis and Photophysical Characterization of Azoheteroarenes, *Org. Lett.*, 2018, **20**(16), 4875–4879.
55 T.-T. Yin, Z.-X. Zhao and H.-X. Zhang, A theoretical study on the thermal cis–trans isomerization of azoheteroarene photoswitches, *New J. Chem.*, 2017, **41**(4), 1659–1669.
56 C. R. Crecca and A. E. Roitberg, Theoretical study of the isomerization mechanism of azobenzene and disubstituted azobenzene derivatives, *J. Phys. Chem. A*, 2006, **110**(26), 8188–8203.
57 L. Gagliardi, G. Orlandi, F. Bernardi, A. Cembran and M. Garavelli, A theoretical study of the lowest electronic states of azobenzene: the role of torsion coordinate in the cis–trans photoisomerization, *Theor. Chem. Acc.*, 2003, **111**(2–6), 363–372.
58 A. Muzdalo, P. Saalfrank, J. Vreede and M. Santer, Cis-to-Trans Isomerization of Azobenzene Derivatives Studied with Transition Path Sampling and Quantum Mechanical/Molecular Mechanical Molecular Dynamics, *J. Chem. Theory Comput.*, 2018, **14**(4), 2042–2051.
59 J. Dokic, M. Gothe, J. Wirth, M. V. Peters, J. Schwarz, S. Hecht and P. Saalfrank, Quantum chemical investigation

of thermal cis-to-trans isomerization of azobenzene derivatives: substituent effects, solvent effects, and comparison to experimental data, *J. Phys. Chem. A*, 2009, **113**(24), 6763–6773.

60 J. Robertus, S. F. Reker, T. C. Pijper, A. Deuzeman, W. R. Browne and B. L. Feringa, Kinetic analysis of the thermal isomerisation pathways in an asymmetric double azobenzene switch, *Phys. Chem. Chem. Phys.*, 2012, **14**(13), 4374–4382.

61 T. Asano, T. Okada, S. Shinkai, K. Shigematsu, Y. Kusano and O. Manabe, Temperature and pressure dependences of thermal cis-to-trans isomerization of azobenzenes which evidence an inversion mechanism, *J. Am. Chem. Soc.*, 2002, **103**(17), 5161–5165.

62 P. R. Huddleston, V. V. Volkov and C. C. Perry, The structural and electronic properties of 3,3′-azothiophene photoswitching systems, *Phys. Chem. Chem. Phys.*, 2019, **21**(3), 1344–1353.

63 S. Devi, M. Saraswat, S. Grewal and S. Venkataramani, Evaluation of Substituent Effect in Z-Isomer Stability of Arylazo-1 H-3,5-dimethylpyrazoles: Interplay of Steric, Electronic Effects and Hydrogen Bonding, *J. Org. Chem.*, 2018, **83**(8), 4307–4322.

64 L. Stricker, M. Bockmann, T. M. Kirse, N. L. Doltsinis and B. J. Ravoo, Arylazopyrazole Photoswitches in Aqueous Solution: Substituent Effects, Photophysical Properties, and Host-Guest Chemistry, *Chemistry*, 2018, **24**(34), 8639–8647.

65 Z. Y. Zhang, Y. He, Y. Zhou, C. Yu, L. Han and T. Li, Pyrazolylazophenyl Ether-Based Photoswitches: Facile Synthesis, (Near-)Quantitative Photoconversion, Long Thermal Half-Life, Easy Functionalization, and Versatile Applications in Light-Responsive Systems, *Chemistry*, 2019, **25**(58), 13402–13410.

66 B. G. Abreha, S. Agarwal, I. Foster, B. Blaiszik and S. A. Lopez, Virtual Excited State Reference for the Discovery of Electronic Materials Database: An Open-Access Resource for Ground and Excited State Properties of Organic Molecules, *J. Phys. Chem. Lett.*, 2019, **10**(21), 6835–6841.

67 S. Batsyts, E. G. Hübner, J. C. Namyslo and A. Schmidt, The Interconnection of Two Positive Charges by Conjugation and Cross–Conjugation in Bis–Quinolinium Ethynyls, *Eur. J. Org. Chem.*, 2019, **2019**(36), 6168–6176.

68 J. Y. C. Ting, R. B. Roseli and E. H. Krenske, How does cross-conjugation influence thiol additions to enones? A computational study of thiol trapping by the naturally occurring divinyl ketones zerumbone and alpha-santonin, *Org. Biomol. Chem.*, 2020, **18**(7), 1426–1435.

69 K. S. Halskov, T. K. Johansen, R. L. Davis, M. Steurer, F. Jensen and K. A. Jorgensen, Cross-trienamines in asymmetric organocatalysis, *J. Am. Chem. Soc.*, 2012, **134**(31), 12943–12946.

70 A. Dieckmann, M. Breugst and K. N. Houk, Zwitterions and unobserved intermediates in organocatalytic Diels-Alder reactions of linear and cross-conjugated trienamines, *J. Am. Chem. Soc.*, 2013, **135**(8), 3237–3242.

71 K. I. Ishiuchi, T. Kubota, S. Hayashi, T. Shibata and J. I. Kobayashi, Lycopladine H, a novel alkaloid with fused-tetracyclic skeleton from Lycopodium complanatum, *Tetrahedron Lett.*, 2009, **50**(47), 6534–6536.

72 D. Li, F. Wang, S. Cai, X. Zeng, X. Xiao, Q. Gu and W. Zhu, Two New Bisorbicillinoids Isolated from a Deep-sea Fungus *Phialocephal*a, sp. FL30r, *J. Antibiot.*, 2007, **60**(5), 317–320.

73 J. Huang, R. Yokoyama, C. Yang and Y. Fukuyama, Structure and Neurotrophic Activity of seco-Prezisaane-Type Sesquiterpenes from Illicium merrillianum, *J. Nat. Prod.*, 2001, **64**, 428–431.

74 V. Schomaker and L. Pauling, The Electron Diffraction Investigation of the Structure of Benzene, Pyridine, Pyrazine, Butadiene-1,3, Cyclopentadiene, Furan, Pyrrole, and Thiophene, *J. Am. Chem. Soc.*, 2002, **61**(7), 1769–1780.

75 D. M. Adrion, D. S. Kaliakin, P. Neal and S. A. Lopez, Benchmarking of Density Functionals for Z-Azoarene Half-Lives via Automated Transition State Search, *J. Phys. Chem. A*, 2021, **125**(29), 6474–6485.

76 M. J. Frisch, G. W. Trucks, H. B. Schlegel, G. E. Scuseria, M. A. Robb, J. R. Cheeseman, G. Scalmani, V. Barone, G. A. Petersson, H. Nakatsuji, X. Li, M. Caricato, A. V. Marenich, J. Bloino, B. G. Janesko, R. Gomperts, B. Mennucci, H. P. Hratchian, J. V. Ortiz, A. F. Izmaylov, J. L. Sonnenberg, D. Williams-Young, F. Ding, F. Lipparini, F. Egidi, J. Goings, B. Peng, A. Petrone, T. Henderson, D. Ranasinghe, V. G. Zakrzewski, J. Gao, N. Rega, G. Zheng, W. Liang, M. Hada, M. Ehara, K. Toyota, R. Fukuda, J. Hasegawa, M. Ishida, T. Nakajima, Y. Honda, O. Kitao, H. Nakai, T. Vreven, K. Throssell, J. A. Montgomery Jr., J. E. Peralta, F. Ogliaro, M. J. Bearpark, J. J. Heyd, E. N. Brothers, K. N. Kudin, V. N. Staroverov, T. A. Keith, R. Kobayashi, J. Normand, K. Raghavachari, A. P. Rendell, J. C. Burant, S. S. Iyengar, J. Tomasi, M. Cossi, J. M. Millam, M. Klene, C. Adamo, R. Cammi, J. W. Ochterski, R. L. Martin, K. Morokuma, O. Farkas, J. B. Foresman and D. J. Fox, *Gaussian 16 Rev. C.01*, Wallingford, CT, 2016.

77 C. Adamo and V. Barone, Toward reliable density functional methods without adjustable parameters: The PBE0 model, *J. Chem. Phys.*, 1999, **110**(13), 6158–6170.

78 R. Ditchfield, W. J. Hehre and J. A. Pople, Self–Consistent Molecular–Orbital Methods. IX. An Extended Gaussian–Type Basis for Molecular–Orbital Studies of Organic Molecules, *J. Chem. Phys.*, 1971, **54**(2), 724–728.

79 F. Furche and R. Ahlrichs, Adiabatic time-dependent density functional methods for excited state properties, *J. Chem. Phys.*, 2002, **117**(16), 7433–7447.

80 J. D. Chai and M. Head-Gordon, Long-range corrected hybrid density functionals with damped atom-atom dispersion corrections, *Phys. Chem. Chem. Phys.*, 2008, **10**(44), 6615–6620.

81 J. Tomasi, B. Mennucci and R. Cammi, Quantum mechanical continuum solvation models, *Chem. Rev.*, 2005, **105**(8), 2999–3093.

